EPJ manuscript No.
(will be inserted by the editor)

The θ_{13} and δ_{CP} sensitivities of the SPL-Fréjus project revisited

Jean Eric Campagne, Antoine Cazes

Laboratoire de l'Accélérateur Linéaire - Université Paris-Sud - Bât. 200 - BP 34 - 91898 Orsay Cedex, France

October 25, 2005

Abstract. An optimization of the CERN SPL beam line has been performed guided by the sensitivities to the θ_{13} mixing angle and to the δ_{CP} Dirac CP violating phase. A UNO-like 440 ktons water Čerenkov detector located at 130 km from the target in a new foreseen Fréjus laboratory has been used as a generic detector. Concerning the δ_{CP} independent θ_{13} sensitivity, a gain of about 20% may be reached using a 3.5 GeV proton beam with a 40 m long, 2 m radius decay tunnel compared to the up to now considered 2.2 GeV beam energy and 20 m long, 1 m radius decay tunnel. This may motivate new machine developments to upgrade the nominal SPL proton beam energy.

1 Introduction

The very near future of the neutrino long baseline experiments is devoted to the study of the oscillation mechanism in the range of $\Delta m^2 = \Delta m^2_{atm} \approx 2.4 \times 10^{-3}\mathrm{eV}^2$ [1,2] using conventional ν_μ beams. The current K2K experiment in Japan [2], and the forthcoming MINOS in the USA [3] take benefit of low energy beam to measure the Δm^2 parameter using the disappearance mode $\nu_\mu \to \nu_\mu$, while OPERA/ICARUS experiments [4,5] using the high energy CNGS beam [6] will be able to detect ν_τ appearance. If we do not consider the LSND anomaly [7] that will be further studied soon by MiniBooNE experiment [8], the three flavor family scenario will be confirmed and accommodated by a 3×3 Pontecorvo-Maki-Nakagawa-Sakata (PMNS) mixing matrix [9] with three angles (θ_{12},θ_{13},θ_{23}) and one Dirac CP phase δ_{CP}.

Beyond this medium term plan, two of the next future tasks of neutrino physics are to improve the sensitivity of the last unknown mixing angle parameter, the so-called θ_{13}, and to explore the CP violation mechanism in the leptonic sector. The present upper bound on θ_{13} is $\sin^2 2\theta_{13} < 0.14$ for $\Delta m^2 = \Delta m^2_{atm}$ (90% CL) [10]. This sensitivity can be improved using reactor and accelerator experiments. In reactor experiments, one uses $\bar{\nu}_e$ in disappearance mode and may reach $\sin^2 2\theta_{13} < 0.024$ for $\Delta m^2 = \Delta m^2_{atm}$ (90%CL) [11]. In accelerator experiments, one can use ν_e and $\bar{\nu}_e$ from β beams [12] in both disappearance and appearance modes (*i.e.* $\overset{(-)}{\nu}_e \to \overset{(-)}{\nu}_\mu$), and also $\overset{(-)}{\nu}_\mu$ in appearance mode (*i.e.* $\overset{(-)}{\nu}_\mu \to \overset{(-)}{\nu}_e$) with conventional beams either with sub-mega watt proton drivers [13,14] or with multi-mega watt proton drivers [14–16]. The later neutrino beam type, called Superbeam, is foreseen to be extended to produce ν_μ beam and $\bar{\nu}_\mu$ beam from muon decays, the so-called Neutrino Factory, in order to study the eventual leptonic CP violation. Such Neutrino Complex is under study in Japan, in USA and also in Europe at CERN and details may be found in reference [16]. A comparison of the performances of β beam and Superbeam may be found for instance in reference [17]. The reactor experiment result on θ_{13} is straight forward as compared to Superbeam and Neutrino Factory results that are on one hand reacher but in an other hand more complex to analyse due to the interplay between the different physics factors θ_{13}, δ_{CP}, sign(Δm^2_{23}), sign($\tan(2\theta_{23})$) [17,18].

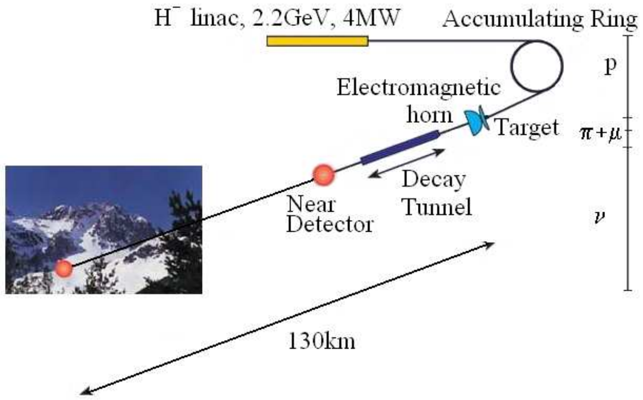

Fig. 1. Sketch of the SPL neutrino Superbeam from CERN to the Fréjus tunnel.

This paper presents results of a new simulation of the SPL (Super Proton Linac) Superbeam that could take place at CERN [19], using for definitiveness a UNO-like 440kT fiducial water Čerenkov detector [20] located in a new enlarged underground laboratory under study in the Fréjus tunnel, 130 km away from CERN [21]. The SPL

Correspondence to: campagne@lal.in2p3.fr

Table 1. Liquid mercury jet parameters.

Hg target	
Hg jet speed	20 m/s
density	13.546
Length, radius	30 cm, 7.5 mm

neutrino beam is created by decays of pions, muons and kaons produced by the interactions of a 4 MW proton beam impinging a liquid mercury jet [16]. Pions, muons and kaons are collected using two concentric electromagnetic lenses (horns), the inner one and the outer one are hereafter called "Horn" and "Reflector" respectively [22]. The horns are followed by a decay tunnel where most of the neutrinos are produced. A sketch of the beam line is shown on figure 1.

The analysis chain consists of different stages: the simulation of the interactions between the proton beam and the mercury target, the propagation of the resulting secondary particles through the magnetic field and the materials of the horns, the tracking of $\pi^{\pm}$, $K^{\pm,0}$ and $\mu^{\pm}$ until they decay, the computation of the neutrino flux at the detector site, and finally the statistical analysis. A part of the simulation chain has already been described in reference [23,24].

Compared to recent papers on the same subject [17, 25,26], we have reoptimized the Horn and Reflector shapes [27], and introduced the kaon background simulation which allows us to update the SPL beam energy. The organization of this document follows the simulation chain: the interaction between the proton beam and the mercury target is presented in the second section. The kaon production is detailed in the third section. The simulation of the horns is described in the forth section, while the algorithms used to compute the neutrino fluxes are explained in the fifth section. Then, the sensitivities to θ_{13} and δ_{CP} are revisited with new studies about the optimization of the proton beam energy, the pion collection and the decay tunnel geometry.

2 Target simulation

Since hadronic processes are crucial to describe the interactions of the proton beam on the target, the FLUKA simulator [28] has been chosen for this first step of the simulation. The target used in the present study is a mercury liquid jet [16] simulated for a sake of simplicity by a cylinder 30 cm long (representing two hadronic lengths) and 1.5 cm diameter (see table 1) [25]. Other types of target are under study [16]. The pencil like simulated proton beam is composed with 10^6 mono-energetic protons, and no beam-target dynamical effects are taken into account. The beam axis is also the symmetry axis of the target and the horns and the decay tunnel. Simulations have been performed for 2.2 GeV proton kinetic energy, the up to now nominal design [19], as well as for 3.5 GeV, 4.5 GeV, 6.5 GeV and 8 GeV according to possible new designs [29].

Particle production yields are summarized in table 2. The pion momentum spectra obtained at different energies and normalized to a 4MW SPL beam power are presented in figure 2(a). At low energy, pions come from Δ decays while the high energy part is dominated with multi pion production. At very mow energy, for $P < 200$ MeV/c, pions come from Δ produced by protons of the target excited by the beam interactions, while for higher energy, pion production is due to transformation of protons of the beam into Δ.

The horns are designed to focus the 600 MeV/c pions (see section 4) and the variation of the number of such pions is rather smooth with respect to the beam energy considering a 4MW fixed beam power: $4.19 \times 10^{13}\pi/\mathrm{s}$ for the 2.2 GeV beam, $4.91 \times 10^{13}\pi/\mathrm{s}$ for the 3.5 GeV beam, $5.14 \times 10^{13}\pi/\mathrm{s}$ for the 4.5 GeV beam, and $4.92 \times 10^{13}\pi/\mathrm{s}$ for the 6.5 GeV beam. The main difference is made by the angular distribution. Figure 2(b) shows this distribution for the π^+ exiting the target with a momentum between 500 MeV/c and 700 MeV/c. The acceptance of the horns is limited to the pion below 25°, and we see that more pions are accepted by the horns for the 3.5 GeV and 4.5 GeV proton beams compared to other beam energies.

The secondary proton and neutron rates induce important radiation damages and power dissipation in the horns which have been addressed in reference [23], and which will require specific R&D effort. At 2.2 GeV, kaon yields are very low, but it has a dramatic energy dependence as further studied in section 3. It is worth to mention that the numbers in table 2 are not to be taken as face values, because the cross sections of pion and kaon productions using proton beam are still under studies as for instance by the HARP experiment [30]. The cross section uncertainties are the main source of discrepancy between simulator programs. Some comparisons between FLUKA and MARS [32] have already been presented in the same context [23]. The energy distribution of the pions exiting the target, computed with the two simulator programs FLUKA and MARS, is shown on figure 3(a). The discrepancy is quite large for the low energy part. However, the horns are designed to focus the high energy part of the spectrum (see section 4), and therefore, MARS and FLUKA are in better agreement for the energy spectrum computed at the entrance of the decay tunnel, as shows figure 3(b). For a 2.2 GeV beam and a positive focusing, 27% more ν_μ and 6% more ν_e neutrinos are produced around the oscillation probability maximum with the FLUKA generator. It turns out that a sensitivity 10% better for FLUKA compared to MARS has been found for the $\sin^2(2\theta_{13})$ sensitivity (see section 7). So, the discrepancy at low energy between MARS and FLUKA does not matter too much for the present application, and the sensitivity difference can be taken as a systematic error.

3 Kaon production

The possibility to increase the SPL energy in order to study the optimization of the physics program has been recently pointed out [29]. Then, the kaon production should

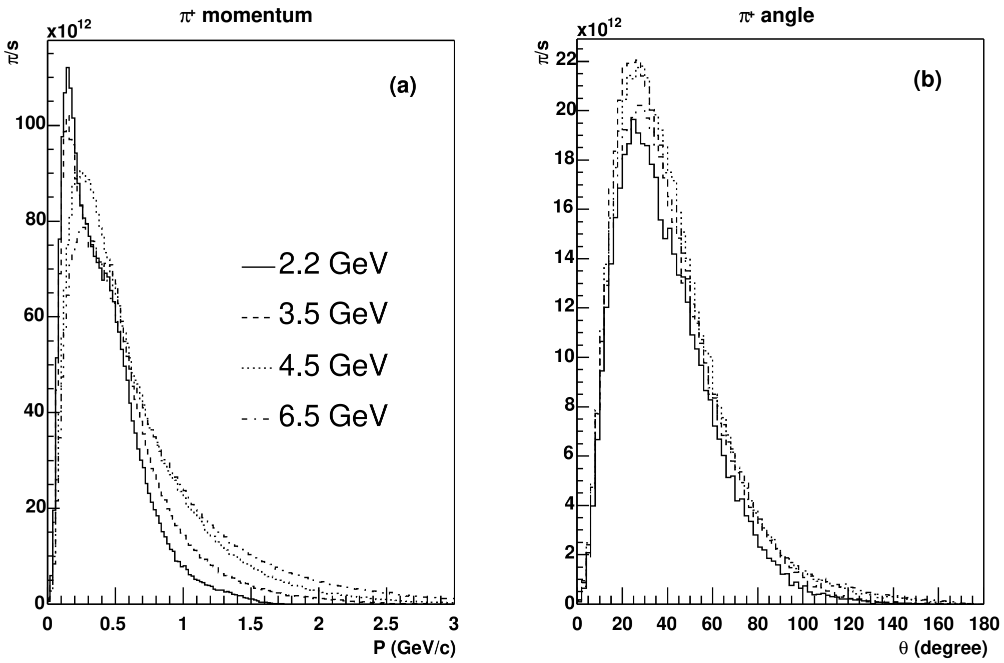

Fig. 2. (a) π^+ momentum distribution per second at the exit of the target for the different proton beam energies studied, simulated with FLUKA, and (b) π^+ angle with respect to the beam axis of the pion having a momentum between 0.5 GeV/c and 0.7 GeV/c. The different SPL beam kinetic energies presented are (——) 2.2 GeV, (- - - -) 3.5 GeV, (······) 4.5 GeV and (— · —) 6.5 GeV

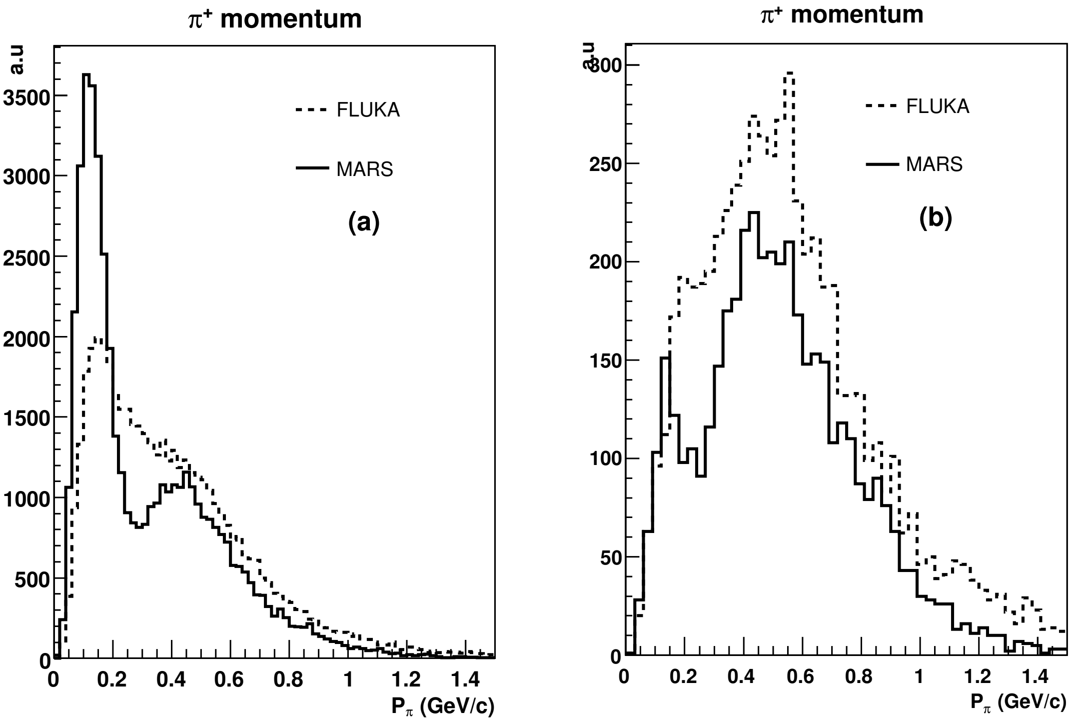

Fig. 3. π^+ momentum distribution at the exit of the target (a) and at the exit of the horns (b), simulated by FLUKA (- - - -) and by MARS (——).

Table 2. Average numbers of the most relevant secondary particles exiting the 30 cm long, 1.5 cm diameter mercury target per incident proton (FLUKA). The μ^+/μ^- numbers and the K^+/K^0 numbers have been multiplied by 10^4. Note that the K^- production rate is at the level of 10^{-5} per incident proton.

E_k (GeV)	p	n	γ	e^+	e^-	π^+	π^-	μ^+	μ^-	K^+	K^0
2.2	1.4	17	5.0	0.08	0.17	0.24	0.18	4	1	7	6
3.5	1.8	23	7.0	0.15	0.28	0.41	0.37	10	3	35	30
4.5	2.3	25	7.7	0.21	0.35	0.57	0.39	11	3.3	93	68
8	3.1	33	11.0	0.41	0.63	1.00	0.85	30	9.5	413	340

be clearly addressed because it is a source of ν_e and $\bar{\nu}_e$ background events. The kaon decay channels and branching ratios are presented in table 14 in A.3.

The target simulation described in section 2 has been used with 10^6 p.o.t with kinetic energy uniformly distributed between 2.2 GeV and 5 GeV. The momentum of outgoing pions and kaons are recorded when they exit the target. The number of produced $K^{o,\pm}$ at different proton beam energies are presented on figure 4 (left). In one hand the K^o production rate is similar to the K^+ production rate, but in an other hand the K^- production rate is almost forty times smaller. For comparison, the numbers of π^+ and π^- produced in the same conditions are presented on figure 4 (right). Pion production rate is about two orders of magnitude greater than the kaon production rate. The behavior of the two pion and kaon production rates are quite different. The π^+ yield grows smoothly with the proton energy while the production of kaons seams to have two origins, which has been confirmed by FLUKA's authors [33]. For beam energy below approximatively 4 GeV, the resonance production model is used, and one notices a low production rate with a maximum at about 3.4 GeV. For beam energy above 4 GeV, the dual parton model is used, and the production rate experiences a threshold effect with a rapid rise. The ratio between positive kaon and pion production rates is about 0.5% between 2.2 GeV and 4 GeV and grow up to 2.3% at 5 GeV. One notices that the transition between the two kaon production models may not be optimal.

4 Horns simulation

The simulation code of the electromagnetic horns is written using GEANT 3.2.1 [34] for convenience and since electromagnetic processes are dominant, FLUKA has not been considered as mandatory, but this may be revised in a future work. The geometry of the horns has been inspired by an existing CERN prototype and a Reflector design proposed in reference [35]. Depending of the current injection, only positive secondary particles or negative secondary particles are focused. The relevant parameters are detailed in table 3.

The mercury target is localized inside the Horn because of the low energy and the large emittance of the secondary pions produced:

$$< P_{\pi T} > / < P_{\pi} > \approx 240 \text{ MeV}/400 \text{ MeV}$$

Table 3. Relevant parameters of the horns in case of the generation of a 260 MeV neutrino beam (or 350 MeV in paranthesis). The shapes of the conductors are independent of the proton beam energy, as the focusing has been optimized for a 600 MeV/c (or 800 MeV/c) pion momentum.

	Horn	Reflector
neck inner radius	3.7 cm	20.3 cm
neck length	40 cm	120(140) cm
end cone inner radius	16 cm	35.7 cm
outer radius	20.3 cm	40 cm
total length	120(140) cm	190(220) cm
Alu thickness	3 mm	3 mm
Peak current	300 kA	600 kA
Frequency	50 Hz	50 Hz

(2.2 GeV proton beam energy). This explains the Horn design (figure 5), with a cylindrical part around the target, called the neck, which is larger than the transversal size of the target to simulate the room for target handling, and a conic part designed such that the relevant pions are focused as much as possible to exit the magnetic field parallel to the beam axis.

The shape of the horn conductors is a crucial point since it determines the energy spectrum of the neutrino at the detector site. The details of the conductor shape optimization for the present context may be found in reference [27]. We just recall here some ingredients. For a θ_{13} driven $\nu_\mu \rightarrow \nu_e$ oscillation, a Δm^2_{23} parameter value of $2.4 \times 10^{-3}\text{eV}^2$, and a baseline distance of 130 km, the first oscillation maximum occurs for a neutrino energy of 260 MeV. The optimization of the physics potential depends at first approximation on the pion neutrino characteristics, which energy is fully determined by the pion 2-body decay and boost. To reach an energy of 260 MeV, the pion needs a $\beta = 0.97$, which in turn induces a pion momentum of 600 MeV/c. Then, the shape of the conic part of the horns is determined such that these 600 MeV/c pions exit parallel to the beam axis.

An other shape of the horn conductors has been used to produce a 350 MeV neutrino beam to compare the sensitivity potential (see section 7). In that case, keeping the current intensity unchanged (300/600 kA), the lengths of the Horn and the Reflector should be increased by 16% and 18.5%, respectively (see table 3).

Before closing this section, it is worth to quote that the Horn/Reflector conductor shapes optimized in the present

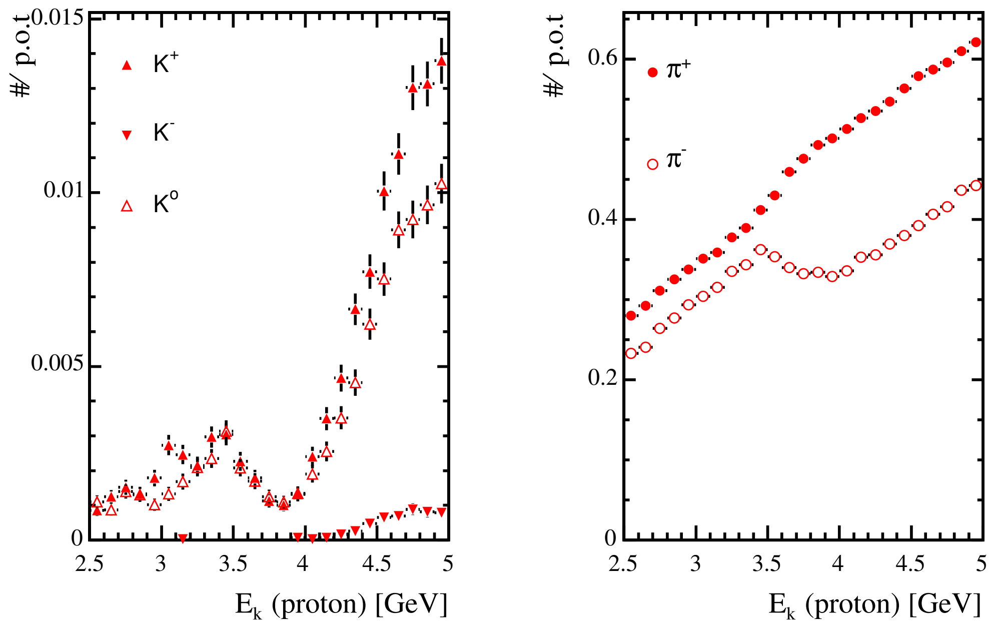

Fig. 4. Kaon production (left panel) and pion production (right panel) defined as number of particle produced per proton on target (p.o.t) as function of the kinetic energy of the incident proton (E_k).

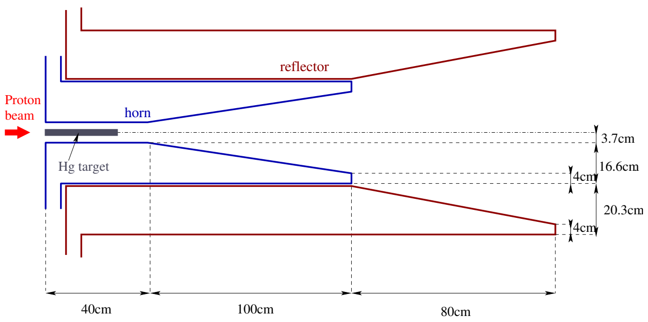

Fig. 5. Design of the Horn and the Reflector conductors implemented in the GEANT simulation in case of the generation of a 350 MeV neutrino beam. The Hg target is located inside the cylindrical part of the Horn.

study to focus a given pion momentum value, is not affected at first order by a proton beam energy change. What is affected is the production rate of the relevant pions. This Horn/Reflector design consideration would be different if one wishes to focus as much as possible all the pions produced for which the mean energy is of course affected by a proton beam energy change.

5 Particle decay treatment and flux calculation

The decay tunnel representation is a simple cylinder with variable length (L_T) and radius (R_T) filled with "vacuum" and located right after the horns. The default design is a 20 m long and 1 m radius cylinder, but simulations have also been conducted with lengths of 10 m, 40 m and 60 m, and radius of 1.5 m and 2 m in the spirit of reference [36]. In the GEANT simulation, to gain in CPU time, only pions, muons and kaons are tracked in the volume of the tunnel, and all particles exiting this volume are discarded.

Beyond the $1/L^2$ solid angle factor due to the source-detector distance (L) which decreases dramatically the fluxes, the neutrino beam focusing is very limited due to the small pion boost factor (≈ 4). Therefore, computational algorithms have been used to avoid a too prohibitive CPU time resulting from the simulation of each secondary particle decay. Otherwise, about 10^{15} p.o.t would have been necessary to obtain reliable statistics for the estimation of the $\bar{\nu}_e$ flux for instance.

It is worth to mention that the particle decays occurring before the entrance of the decay tunnel are also taken into account and treated in the same manner, which is not the case in reference [36].

5.1 Algorithm description

The decay code has been included in the GEANT code. The basic idea of this algorithm is to compute the neutrino fluxes using the probability of reaching the detector for each neutrino produced by a π or a K or a μ particle (on-axis neutrino beam). This method has already been used in reference [36] and has been modified and extended to the kaon decay chain for the present study.

Muon neutrino comes mostly from pion decay. In a first stage, each pion is tracked by GEANT until it decays.

Table 4. Number of protons on target for different beam energy at 4 MW constant power. One year is defined as 10^7 s.

Beam energy (GeV)	Number of proton per year (10^{23} p.o.t/y)
2.2	1.10
3.5	0.70
4.5	0.56
6.5	0.40
8.0	0.30

Then, the probability for the produced muon neutrino to reach the detector is computed. The flux is obtained applying the probability as a weight for each neutrino. All the pions produced in the simulation are therefore useful to compute the flux, and this allows to reduce the number of events in the simulation to 10^6 p.o.t. In this computation, the decay region (horns and tunnel) is considered as point like compared to the source-detector distance.

The same method is applied for neutrino coming from muons and kaons with some modifications because most of the muons do not decay, and there are very few kaons produced (see table 2). The probability computation is presented in appendix A.

5.2 Validation of the algorithm

The validity of the method presented in the previous section have been tested against a straight forward algorithm consisting of decaying each pion N times ($N \approx 10^6$) in a full GEANT simulation of the event (decays included). Such method presents the advantage to keep all the information of the neutrino available for further studies. It can be a good approach to compute the muon neutrino flux coming from pion decays. It can also provide the beam profile, but it shows its limits for the muon induced fluxes, especially the $\bar{\nu}_e$ flux. Indeed, this means that each muon is duplicated N times and when a muon decays, it must decay N times again. For $N \approx 10^6$, this is a prohibitive CPU time consuming. The ν_μ and $\bar{\nu}_\mu$ fluxes are displayed on figure 12 for both methods. The two spectra shows a clear agreement, and this makes confidence on the probability method.

5.3 Simulated fluxes

The fluxes are computed at a distance of 100 km from the source by convention and can be rescaled at any desired distance. They provide the number of the four neutrino species (ν_μ, $\bar{\nu}_\mu$, ν_e, $\bar{\nu}_e$) passing through a 100 m^2 fiducial area during 1 year.

In practice, the fluxes are given as a function of the neutrino energy via histograms composed of 20 MeV bin width. These histograms are filled with the energy of each neutrino weighted by the probability to reach the detector (section 5.1). To obtain the fluxes, the histograms are rescaled to the number of p.o.t per year depending on the beam energy. Table 4 reports on the number of p.o.t per year for the different energies studied using the definition of one year being 10^7 s and keeping the beam power constant (*i.e.* 4 MW).

Three origins are identified in the composition of each neutrino flux:

- neutrinos from pions, which includes neutrinos created by primary pion decays and neutrinos coming from the muons produced by pion decays or muons directly exiting the target. This is the component studied in reference [36] but with different settings and event generator;
- neutrinos emitted during the decay chain of the charged kaons, either by direct production, or produced by the daughter pions and muons;
- neutrinos coming from the decay chain of the neutral kaons.

The three components of the fluxes for the four neutrino species are presented on figure 6 for positive particle focusing and a proton beam kinetic energy of 2.2 GeV. The ν_μ flux is dominated by the neutrinos of pion decays, but a tail above 500 MeV (insert on the top left part) is created by the $K^+ \to \mu^+\nu_\mu$ channel, which is anyway at least three order of magnitude below the flux maximum. The $\bar{\nu}_\mu$ flux is mostly due to the decays of π^- that are not unfocused by the horns, but the higher energy part comes from μ^+ decays. It is noticable that the ν_e and $\bar{\nu}_e$ fluxes are respectively more than 200 and more than 7000 times smaller than the ν_μ flux. The $\bar{\nu}_e$ are produced in a large part by the $K^0_L \to \pi^+e^-\bar{\nu}_e$ decay channel and by μ^- decays, while the ν_e flux is dominated by the μ^+ decays.

On figure 7, the horns are set to focus negative particles keeping other parameters identical. By comparison with positive focusing, one can at first approximation translate the results by exchanging particles and anti-particles, except that the K^+/K^- ratio is about 50 in the beam-target interactions (see table 2).

On figures 8 and 10, one observes the evolution of figure 6 when the proton beam kinetic energy increases to 3.5 GeV and 8 GeV, respectively. Correspondingly, the results for negative particle focusing are presented on figures 9 and 11. One clearly notices the increase of the kaon induced neutrino contents as the beam energy grows. On table 5 are reported the integral of the fluxes when one modifies the decay tunnel length and radius, as well as the beam kinetic energy. Changing the length from 10 m to 40 m will increase the ν_μ flux by 50% to 70% and in the same time, the number of ν_e will be multiply by a factor 1.5 to 2. One can notice that going from 40 m to 60 m does not increase the signal-like events but increase the background-like events. For a 40 m length of the decay tunnel, the increase of the radius improve the number of signal-like events by 50%, and the backgroud increase by 70% to 100%. Notice that the $\nu_\mu/\bar{\nu}_\mu$ flux ratio is rather insensitive to the decay tunnel length. The feeling that $L_T = 40$ m and $R_T = 2$ m is a good signal over background compromise is confirmed by sensitivity quantitative studies reported in section 7.

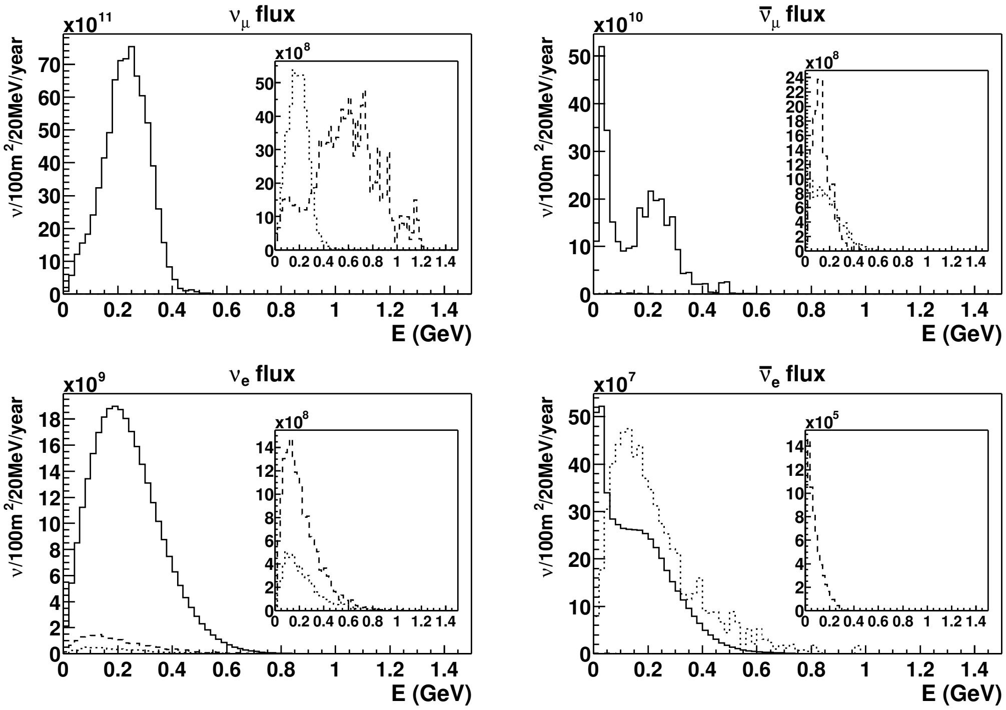

Fig. 6. Neutrino fluxes, 100 km from the target and with the horns focusing the positive particles. The fluxes are computed for a SPL proton beam of 2.2 GeV (4 MW), a decay tunnel with a length of 20 m and a radius of 1 m. The top left panel contains the ν_μ fluxes, and the top right panel shows the $\bar{\nu}_\mu$ fluxes. The bottom left panel presents the ν_e fluxes while the bottom right panel displays the $\bar{\nu}_e$ fluxes. The (——) curve is the contribution from primary pions and the daughter muons, and from primary muons. The (- - - -) curve is the contribution from the charged kaon decay chain, and the (⋯⋯) curve is the contribution from the K^0 decay chain. An insert has been added to the plots to hight light when needed the contribution of charged and neutral kaons.

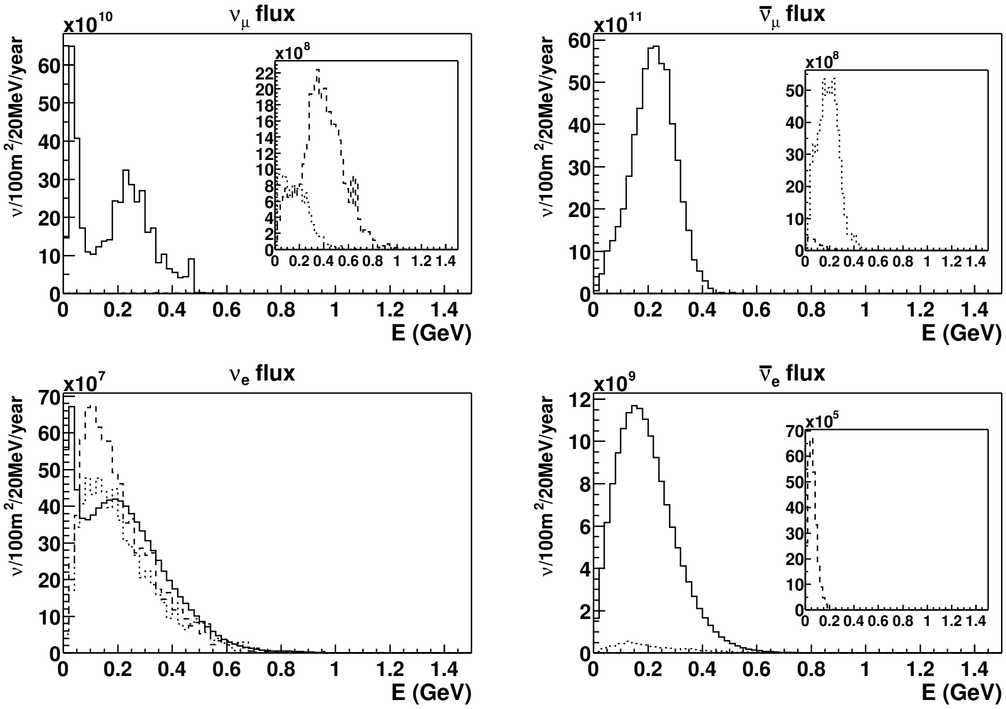

Fig. 7. Same legend as for figure 6 but the horns are focusing negative particles.

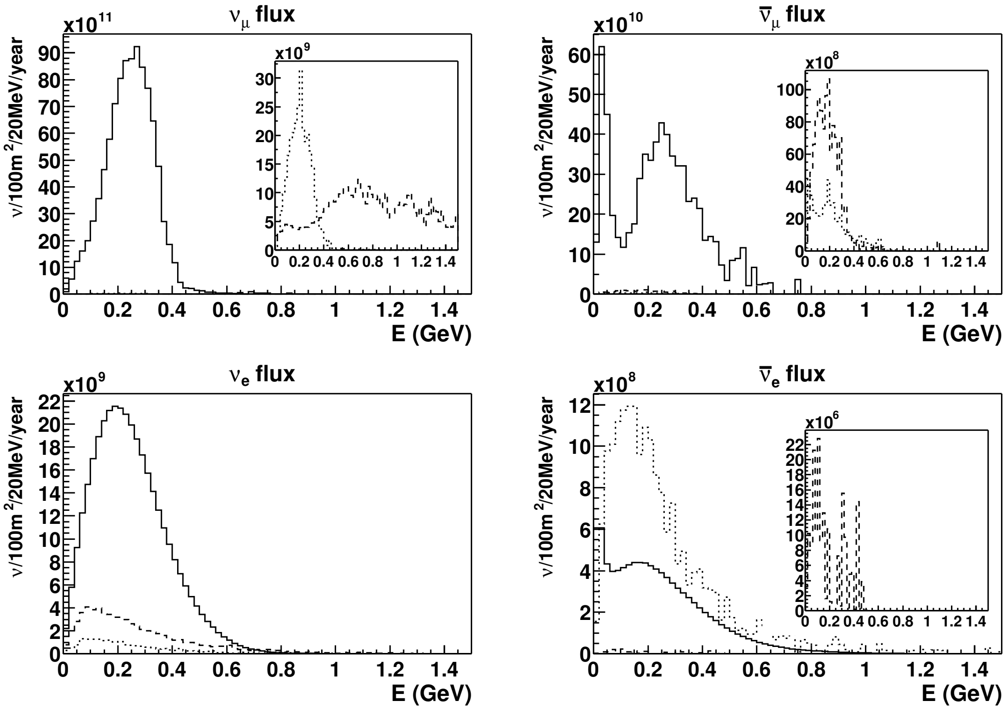

Fig. 8. Same legend as for figure 6 but for proton beam kinetic energy of 3.5 GeV (4 MW).

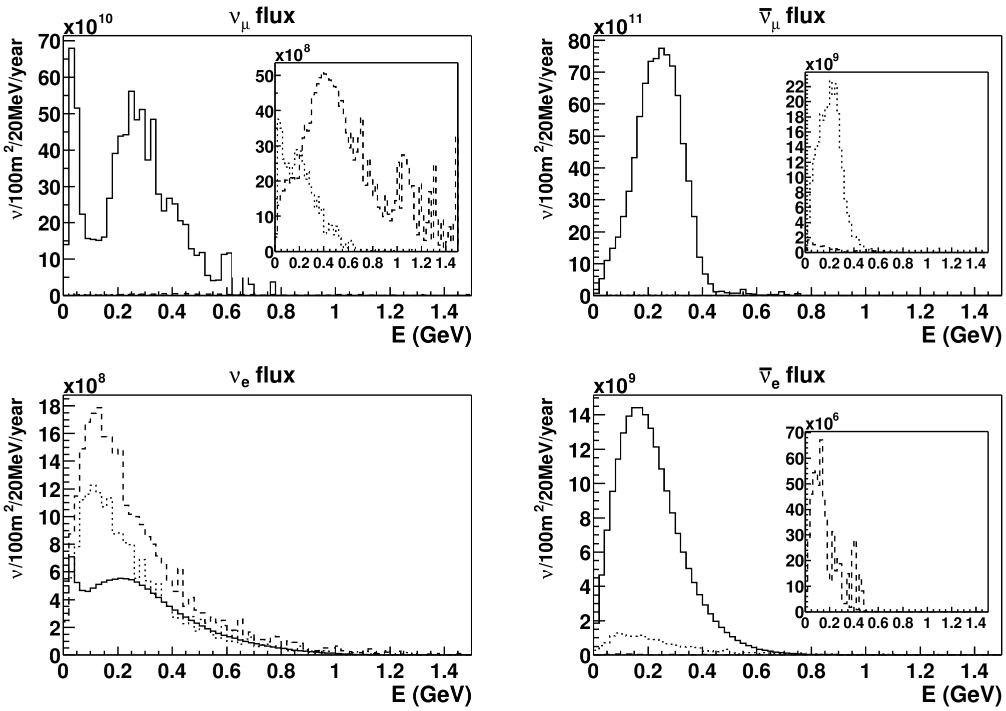

Fig. 9. Same legend as for figure 7 but for proton beam kinetic energy of 3.5 GeV (4 MW).

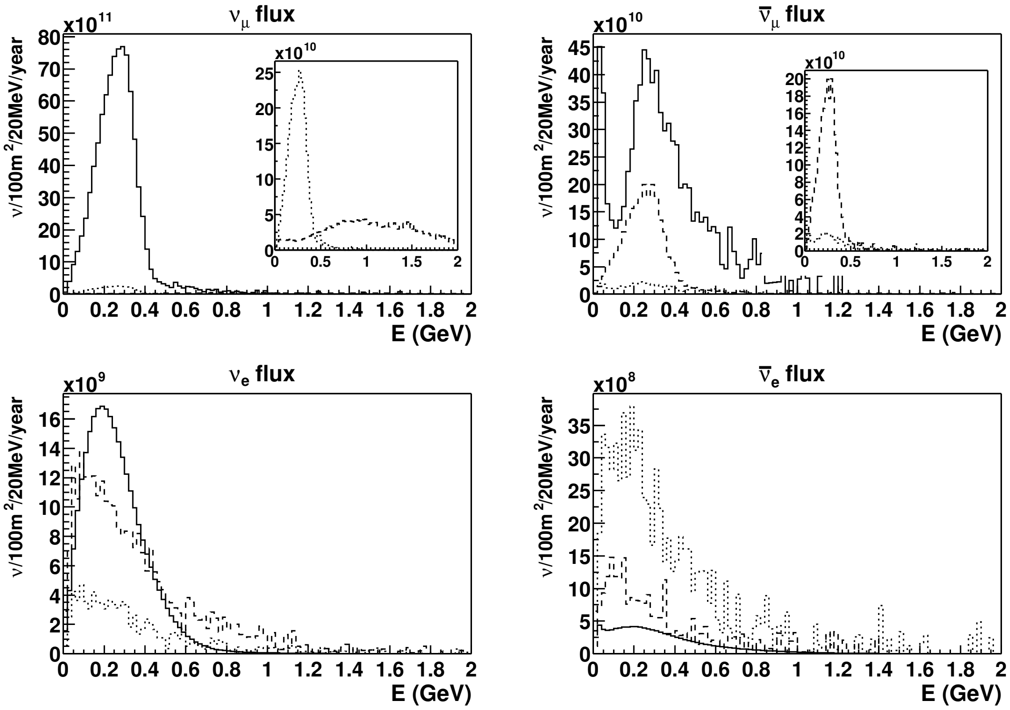

Fig. 10. Same legend as for figure 6 but for proton beam kinetic energy of 8 GeV (4 MW).

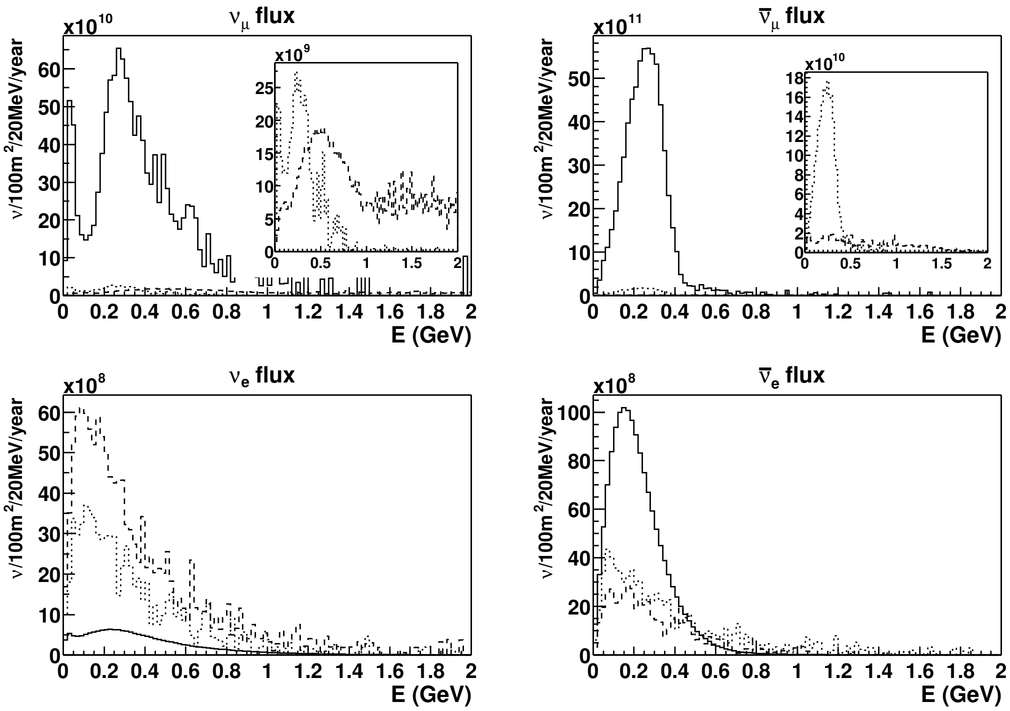

Fig. 11. Same legend as for figure 7 but for proton beam kinetic energy of 8 GeV (4 MW).

Table 5. Integral of the total flux of the different species with different settings. The ν_μ and $\bar{\nu}_\mu$ fluxes are expressed in $10^{13}/100\text{m}^2/y$ unit while the ν_e and $\bar{\nu}_e$ fluxes are expressed in $10^{11}/100\text{m}^2/y$ unit. The positive focusing and negative focusing are distinguished by a (+) sign and a (−) sign, respectively. The settings used corresponds to different values of L_T and R_T, the length and radius of the decay tunnel.

	Settings		ν_μ		ν_e		$\bar{\nu}_\mu$		$\bar{\nu}_e$	
E_p	L_T	R_T	+	−	+	−	+	−	+	−
2.2 GeV	10 m	1 m	5.5	0.4	1.7	0.2	0.3	4.3	0.1	0.8
3.5 GeV	10 m	1 m	7.7	0.7	2.6	0.6	0.6	6.6	0.3	1.3
4.5 GeV	10 m	1 m	7.1	1.0	2.8	0.9	0.5	5.2	0.3	1.1
6.5 GeV	10 m	1 m	8.3	1.2	4.7	1.9	0.8	5.6	0.9	1.8
8.0 GeV	10 m	1 m	7.7	1.2	5.1	2.2	0.9	5.6	1.1	2.1
2.2 GeV	20 m	1 m	7.6	0.4	3.2	0.2	0.3	5.8	0.1	1.6
3.5 GeV	20 m	1 m	10.0	0.9	4.4	0.6	0.7	8.5	0.3	2.2
4.5 GeV	20 m	1 m	10.9	1.1	5.1	1.0	0.7	6.7	0.4	1.8
6.5 GeV	20 m	1 m	10.4	1.4	6.4	2.0	1.0	7.1	0.9	2.5
8.0 GeV	20 m	1 m	9.7	1.5	6.7	2.3	1.2	7.1	1.1	2.8
2.2 GeV	20 m	1.5 m	9.0	0.6	4.4	0.4	0.4	6.7	0.2	2.2
4.5 GeV	20 m	1.5 m	13.2	1.5	6.9	1.4	0.9	8.1	0.6	2.7
3.5 GeV	30 m	1 m	10.9	0.9	5.7	0.7	0.7	9.4	0.3	2.9
4.5 GeV	30 m	1 m	11.6	1.2	6.3	1.0	0.7	7.1	0.4	2.3
2.2 GeV	40 m	1 m	8.9	0.5	5.1	0.3	0.5	6.7	0.1	2.4
3.5 GeV	40 m	1 m	11.3	0.9	6.5	0.6	0.8	9.7	0.3	3.3
4.5 GeV	40 m	1 m	12.3	1.2	7.2	1.0	0.8	7.5	0.4	2.6
6.5 GeV	40 m	1 m	11.7	1.6	8.3	2.2	1.1	8.0	0.9	3.3
8.0 GeV	40 m	1 m	10.9	1.7	8.5	2.4	1.3	8.0	1.2	3.6
3.5 GeV	40 m	1.5 m	14.5	1.3	10.0	1.0	1.0	12.3	0.5	5.3
4.5 GeV	40 m	1.5 m	15.5	1.7	10.8	1.5	1.0	9.5	0.6	4.2
3.5 GeV	40 m	2 m	16.6	1.5	12.9	1.3	1.3	13.9	0.7	6.9
4.5 GeV	40 m	2 m	18.2	2.1	14.3	1.9	1.3	11.1	0.8	5.6
3.5 GeV	60 m	1 m	11.7	0.9	7.6	0.7	0.7	10.1	0.3	3.7
4.5 GeV	60 m	1 m	12.5	1.3	8.1	1.1	0.7	7.7	0.4	2.9
3.5 GeV	60 m	1.5 m	15.1	1.3	12.2	1.0	1.0	12.8	0.5	6.3
4.5 GeV	60 m	1.5 m	16.2	1.8	13.1	1.6	1.0	9.9	0.6	4.9

Looking at the evolution of ν_μ flux with respect to the beam energy, one notices that a maximum is reached around 4.5 GeV. This is due to the competition between the cross section rise with respect to the energy and the decrease of the number of p.o.t due to the constant SPL power (4 MW).

6 Sensitivity computation ingredients

The sensitivity to θ_{13} and δ_{CP} is computed for a $\nu_\mu \to \nu_e$ appearance experiment. The detector considered for definitiveness is similar to the UNO detector, *i.e.* a 440 kt fiducial water Čerenkov detector [20]. The detector simulation has been presented in reference [25] and the analysis program described in reference [37] has been used for sensitivity computation following previous work of reference [26]. See table 6 for the default user parameter values used in this paper. We just remind here some key points of the sensitivity analysis program.

It is included a full 3-flavors oscillation probability computation with matter effects, but no ambiguities are taken into account. This latest point may be revisited in a future work using reference [38]. Concerning the background events, the $\nu_e/\bar{\nu}_e$ from the beam, the $\nu_\mu e^-$ elastic scattering process, the π^o production as well as the μ/e misidentification are taken into account. The cross-sections from the NUANCE program are used [39]. The systematics error on the total ν_e and $\bar{\nu}_e$ fluxes determination is a user parameter and we have used the 2% value considered as a final goal, but also 5% and 10% [37]. The detector is located at $L = 130$ km from CERN, in the foreseen new Fréjus laboratory [21]. It is worth to mention that if one wants to evaluate the influence of L on the sensitivity, it would mean a re-optimization of the horns for each L envisaged (see section 4). The running time scenario has been fixed either by focusing positive particles during 5 years, either by focusing positive particles during 1 (or 2) year(s) followed by focusing negative particles during 4 (or 8) years.

7 Results

7.1 The positive only focusing scenario

The θ_{13} and δ_{CP} sensitivities are computed with $\theta_{13} = 0°$ and $\delta_{CP} = 0°$ if not explicitly mentioned. It is worth to stress that the default parameters of table 6 are used if not contrary mentioned, in particular, the decay tunnel

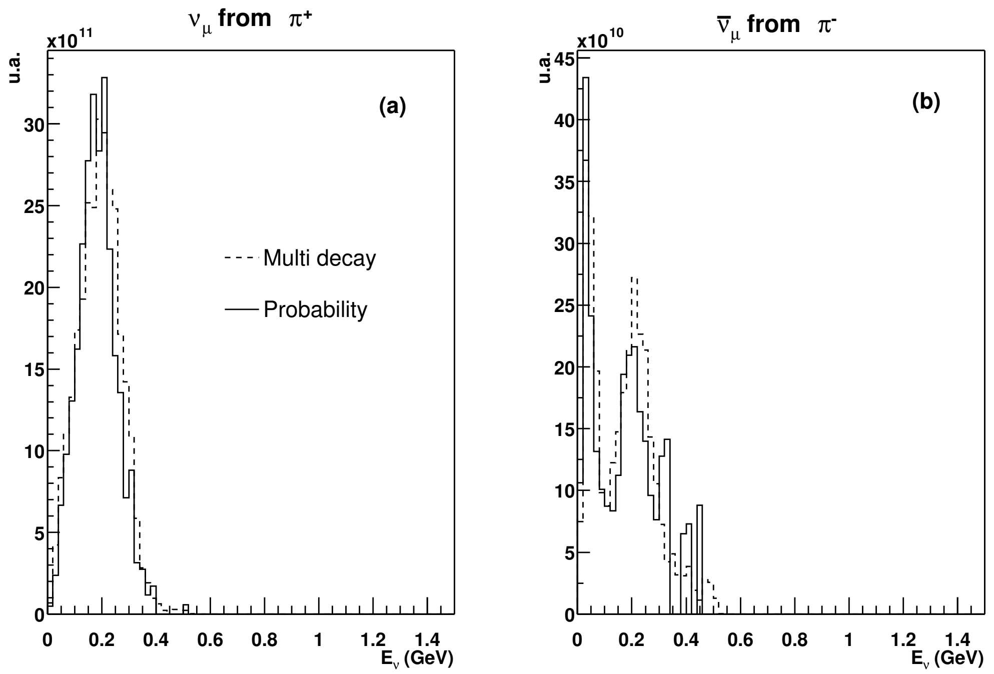

Fig. 12. Comparison between the probability method, (——) curve, and the full GEANT simulation method, (- - - -) curve, for the ν_μ from π^+ flux (a) and the $\bar{\nu}_\mu$ from π^- flux (b). The horns are set to focus positive particles. It should be stressed that the full GEANT simulation has taken roughly 13 times more CPU time than the probability method with the same number of protons on target, and the later simulation is able to produce as well the ν_e and $\bar{\nu}_e$ fluxes contrary to the former simulation.

Table 6. Default parameters used to compute the sensitivity curves [37]. The quoted errors in parenthesis for the (12) and the (23) parameters (absolute value for the masse square differences and relative value for the angles) are coming respectively from the up to date combined Solar and KamLAND results [40] and from a 200 ktons-years SPL desappearance exposure [25].

$\Delta m^2_{12} = 8.2(0.5) \times 10^{-5}$ eV^2	$\sin^2 2\theta_{12} = 0.82(9\%)$
$\Delta m^2_{23} = 2.5(0.1) \times 10^{-3}$ eV^2	$\sin^2 2\theta_{23} = 1.0(1\%)$
$L_T = 20$ m	$R_T = 1$ m
$M = 440$ kT	$\epsilon_{syst} = 2\%$
Horn/Reflector shapes to produce a 260 MeV neutrino beam	

geometry parameters ($L_T = 20$ m and $R_T = 1$ m), and the horn design to generate a 260 MeV neutrino beam.

Table 7 presents the number of signal and background events for a 5 years positive focusing experiment, but with different beam energy settings. The contours at 90%, 95% and 99% CL of the θ_{13} sensitivity are presented in the ($\sin^2 2\theta_{13}$, Δm^2_{23}) plane on figure 13 for 3.5 GeV proton beam kinetic energy. The comparison between the contours at 90% CL with 2.2 GeV, 3.5 GeV, 4.5 GeV and 8 GeV beam energies is shown on figure 14. One notices in this scenario a better perfomence reached with a 4.5 GeV energy beam. But, in fact there is not much visual difference between a sensitivity obtained with 3.5 GeV and 4.5 GeV, even if one should keep in mind that kaon production models are different at these two energies (see section 3). These two energy settings have been studied with different decay tunnel geometry and results are reported on table 9. One notice that similar results can be reached with a 3.5 GeV beam, compared to a 4.5 GeV beam.

Quantitative studies of the minimum $\sin^2 2\theta_{13}$ with respect to the kinetic beam energy $E_k(proton)$, and the decay length L_T, and the systematics ϵ_{syst} are presented in tables 8 and 10. One notices that for $\epsilon_{syst} = 5\%$ there is no difference between a 3.5 GeV and a 4.5 GeV beam. We have also considered the 3.5 GeV and 4.5 GeV beam energies with the tunnel geometry parameters $L_T = 40$ m and $R_T = 2$ m, and the horn design producing a 350 MeV neutrino beam (see section 4). In table 9 are reported numerical values, and on figure 15 are shown the 90% CL sensitivity contours. With the 350 MeV neutrino beam, one can expect a 16% improvment with respect to the 260 MeV neutrino beam. One notices also that there is marginal gain to increase the beam energy from 3.5 GeV to 4.5 GeV, as already mentioned.

There are also variations on the minimum $\sin^2 2\theta_{13}$ value that may be reached in a $\nu_\mu \to \nu_e$ experiment which are due to the sign(Δm^2_{23}) ambiguity and the δ_{CP} value. On table 11 are presented these kind of variations. Other ambiguities coming from the sign($\tan(2\theta_{23})$) ignorance also take place as studied in reference [17]. From figure 9 of this reference, we estimate a 30% effect on $\sin^2(2\theta_{13})$ sensivity due to these ambiguities.

Table 7. Number of events for 5 years positive focusing scenario with default parameters of table 6. Other backgrounds are π^0, ν_μ-elast., μ/e-missId.

	2.2 GeV	3.5 GeV	4.5 GeV	6.5 GeV	8 GeV
non oscillated ν_μ	36917	60969	73202	78024	76068
oscillated ν_e	43	60	64	61	56
beam ν_e	165	222	242	288	299
other background	70	105	127	148	152

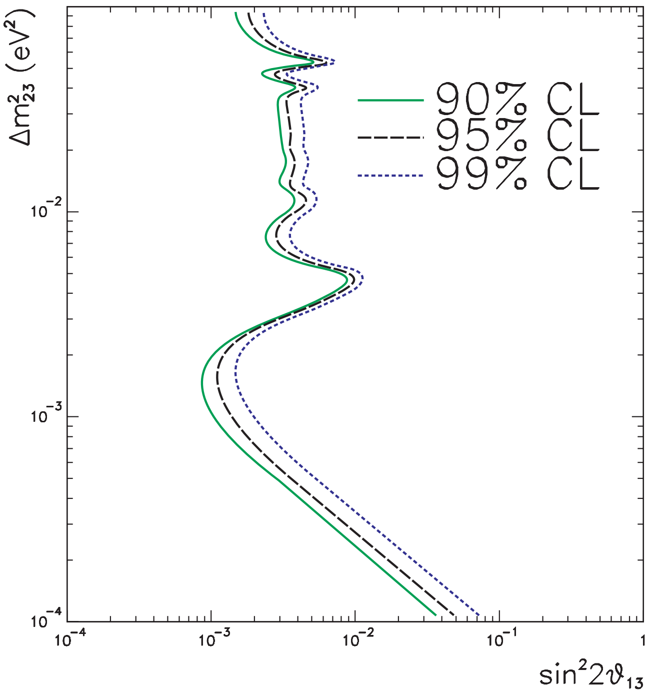

Fig. 13. Sensitivity contours obtained with a SPL energy of 3.5 GeV and default parameters of table 6. In particular, it is reminded that the tunnel geometry parameters are $L_T = 20$ m and $R_T = 1$ m. (——), (- - - -) and (······) curves stand for 90%, 95% and 99% confidence level, respectively.

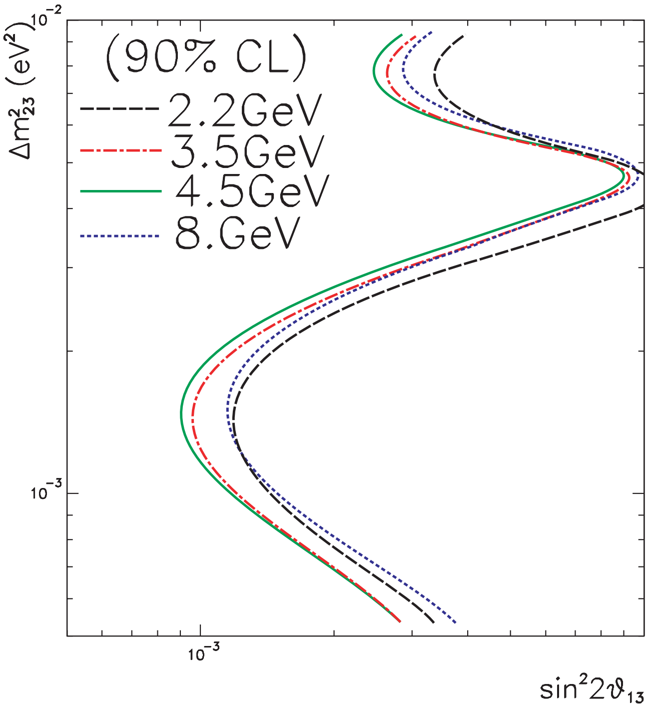

Fig. 14. Comparison of 90% CL sensitivity contours obtained with SPL energies of 2.2 GeV (- - - -), 3.5 GeV (— · —), 4.5 GeV (——) and 8 GeV (······) and default parameters of table 6. In particular, it is reminded that the tunnel geometry parameters are $L_T = 20$ m and $R_T = 1$ m.

Table 8. Minimum $\sin^2 2\theta_{13} \times 10^3$ in the $(\sin^2 2\theta_{13}, \Delta m^2_{23})$ plane observable at 90% CL computed for different decay tunnel length (L_T) and kinetic beam energy ($E_k(proton)$) and 5 year of positive focusing. Other parameters are fixed to default values (table 6).

	2.2 GeV	3.5 GeV	4.5 GeV	6.5 GeV	8 GeV
10 m	1.10	0.92	1.04	1.07	1.16
20 m	1.16	0.92	0.89	1.01	1.12
40 m	1.23	1.00	0.99	1.08	1.19

7.2 Mixed positive/negative focusing scenario

The combined $\sin^2 2\theta_{13}$ and δ_{CP} sensitivity for the 5 years positive focusing scenario and the default parameters of table 6 is presented on figure 16(a). The results obtained with a 3.5 GeV and 4.5 GeV SPL beam are similar and better than with the other energy settings. On figure 17(a) the results obtained with a 260 MeV neutrino beam and a 350 MeV neutrino beam are presented with a 40 m long, 2 m radius decay tunnel. With the 350 MeV neutrino beam, one can reached better sensitivity results in the range $|\delta_{CP}| < 120^o$, and comparatively the gain obtained when switching from a 3.5 GeV proton beam to a 4.5 GeV proton beam is marginal. To improve the δ_{CP}-independent limit on $\sin^2 2\theta_{13}$, especially around $\delta_{CP} = 90°$, one may envisaged a combination of 2 years with positive focusing and 8 years negative focusing as in references [17,25,26]. The comparison of the results obtained with different SPL beam energies on the combined sensitivity contours are presented in figure 16(b). Quantitative results with this kind of mixed focusing scenario are reported table 12. One generally gets 10% to 20% better limit on $\sin^2 2\theta_{13}$ independently of δ_{CP} with a 3.5 GeV kinetic energy beam compare to a 2.2 GeV beam. Doubling the length and the radius of the decay tunnel allows to reach a 10% better limit.

Table 9. Minimum $\sin^2 2\theta_{13} \times 10^3$ in the $(\sin^2 2\theta_{13}, \Delta m^2_{23})$ plane observable at 90% CL computed for different decay tunnel length (L_T) at and radius (R_T) for the 3.5 GeV and 4.5 GeV scenarios and 5 years of positive focusing. Other parameters are fixed to default values (table 6). Settings in parenthesis are identical to those of table 5, except that the setting (7b) corresponds to the tunnel geometry of setting (7) but the horn geometry producing a 350 MeV neutrino beam is used. We remind that the setting (2) is the default one, and the settings (7) and (7b) corresponds to $L_T = 40$ m and $R_T = 2$ m.

setting	(1)	(2)	(3)	(4)	(5)	(6)	(7)	(7b)	(8)	(9)
3.5 GeV	0.92	0.92	0.83	0.98	1.00	0.93	0.91	0.76	1.05	1.01
4.5 GeV	1.04	0.89	0.82	0.94	0.99	0.92	0.87	0.71	1.03	1.00

Table 12. Minimum $\sin^2 2\theta_{13} \times 10^3$ observable at 90% CL computed for the worse δ_{CP} case, and for different decay tunnel length (L_T) and radius (R_T) for the 3.5 GeV and 4.5 GeV scenarios and 2 years of positive focusing plus 8 years of negative focusing. Other parameters are fixed to default values (table 6). Settings are identical to those of table 5.

setting	(1)	(2)	(3)	(4)	(5)	(6)	(7)	(7b)	(8)	(9)
2.2 GeV		2.52			2.58		2.30			
3.5 GeV	2.34	2.22	2.10	2.13	2.09	2.08	2.02	2.28	2.16	2.09
4.5 GeV	2.91	2.60	2.43	2.48	2.52	2.39	2.34	2.55	2.53	2.47

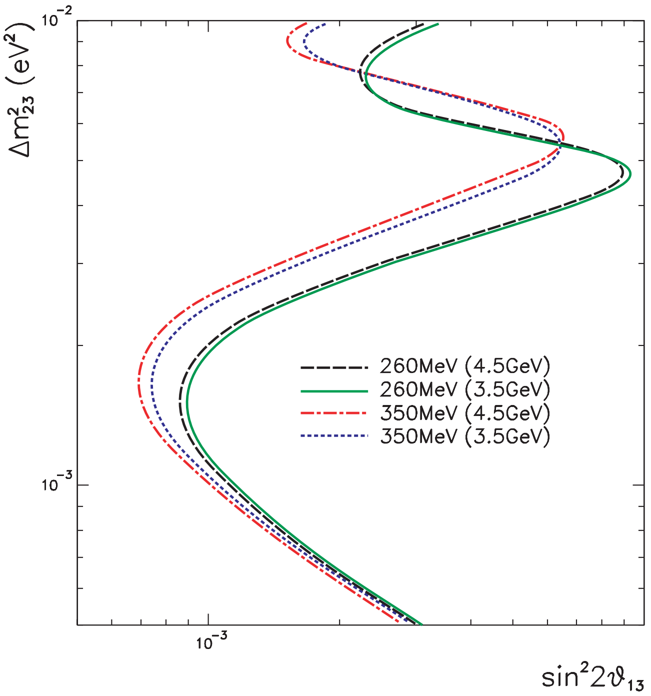

Fig. 15. Comparison of 90% CL sensitivity contours obtained with SPL energies of 3.5 GeV or 4.5 GeV, and either a 260 MeV (default) neutrino beam or a 350 MeV neutrino beam. The tunnel geometry parameters are $L_T = 40$ m and $R_T = 2$ m. The (— · —) curve corresponds to a 350 MeV/4.5 GeV (neutrino beam/SPL beam energy) setting; the (· · · · · ·) curve corresponds to a 350 MeV/3.5 GeV setting; the (- - - -) curve corresponds to a 260 MeV/4.5 GeV setting and the (——) curve corresponds to a 260 MeV/3.5 GeV setting.

On figure 17(b) are presented the results considering the effects of a 350 MeV neutrino beam obtained either with a 3.5 GeV proton beam or a 4.5 GeV proton beam compared to a 260 MeV neutrino beam obtained with a 4.5 GeV proton beam. The tunnel geometry parameters are $L_T = 40$ m and $R_T = 2$ m (other tunnel geometry have been studied but the results are worse and so are not reported). Except in the region $|\delta_{CP}| > 150^o$, the results obtained with the 350 MeV neutrino beam (3.5 GeV proton beam) are somewhat better, even if a 11% improvement of the δ_{CP}-independent $\sin^2 2\theta_{13}$ limit can be reached with the 260 MeV neutrino beam obtained with the 3.5 GeV proton beam.

Table 10. Minimum $\sin^2 2\theta_{13} \times 10^3$ in the $(\sin^2 2\theta_{13}, \Delta m^2_{23})$ plane observable at 90% CL computed for different level of systematics (ϵ_{syst}) and kinetic beam energy ($E_k(proton)$) and 5 years of positive focusing. Other parameters are fixed to default values (table 6).

	2.2 GeV	3.5 GeV	4.5 GeV	6.5 GeV	8 GeV
2%	1.16	0.92	0.89	1.01	1.12
5%	1.48	1.25	1.25	1.48	1.64
10%	2.40	2.14	2.21	2.72	3.09

Table 11. Minimum $\sin^2 2\theta_{13} \times 10^3$ in the $(\sin^2 2\theta_{13}, \Delta m^2_{23})$ plane observable at 90% CL computed for a 2.2 GeV kinetic energy proton beam, and for different values of sign(Δm^2_{23}) and δ_{CP} and 5 years of positive focusing. Other parameters are fixed to default values (table 6).

	$-180°$	$-90°$	$0°$	$90°$	$180°$
+	1.40	0.43	1.16	11.48	1.40
−	1.45	11.75	1.11	0.43	1.45

8 Summary and outlook

A complete chain of simulation has been set up for the SPL-Fréjus project. The neutrino production has been extended to the kaon decay contribution, which is important to test SPL energy scenario above 2.2 GeV. The beam line

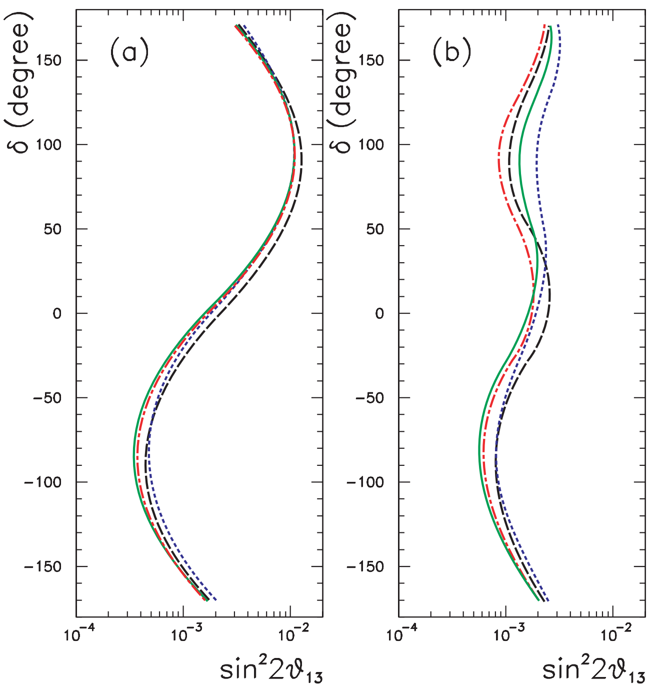

Fig. 16. 90% sensitivity contours obtained with SPL beam energy of 2.2 GeV (- - - -), 3.5 GeV (— · —), 4.5 GeV (——) and 8 GeV (······) at 90% CL. Default parameters of table 6 are used either with a 5 years positive focusing scenario (a) or a mixed scenario of 2 years positive focusing and 8 years of negative focusing (b). In particular, it is reminded that the tunnel geometry parameters are $L_T = 20$ m and $R_T = 1$ m.

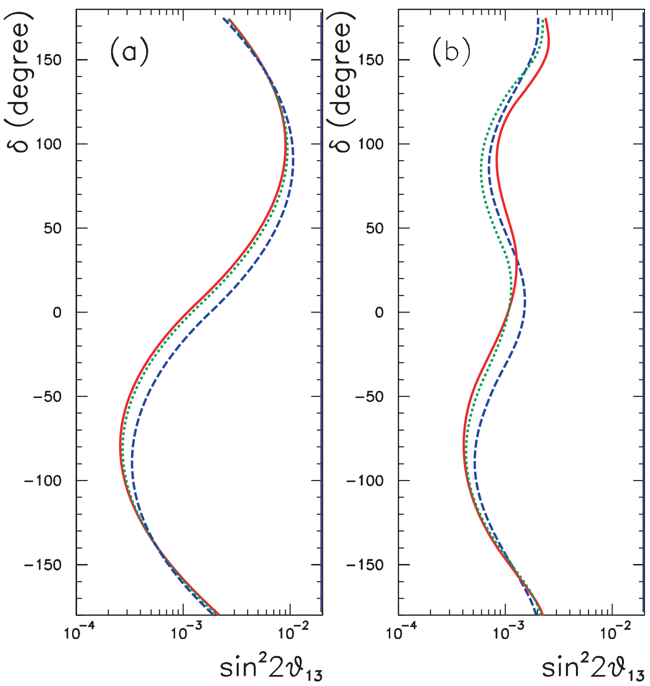

Fig. 17. 90% CL sensitivity contours obtained with the decay tunnel geometry parameters $L_T = 40$ m and $R_T = 2$ m and different SPL beam energies (3.5 GeV or 4.5 GeV) and different horn designs (260 MeV or 350 MeV neutrino beams): (——) curve for a 350 MeV/4.5 GeV setting, (······) curve for a 350 MeV/3.5 GeV setting, (- - - -) curve for a 260 MeV/3.5 GeV setting. Other default parameters of table 6 are used either with a 5 years positive focusing scenario (a) or a mixed scenario of 2 years positive focusing and 8 years of negative focusing (b).

optimization has been performed using the sensitivity to $\sin^2 2\theta_{13}$ and δ_{CP}. The shape of the focusing system has been updated to obtain a neutrino beam energy around 260 MeV or 350 MeV.

In a positive only focusing scenario, the best limit on $\sin^2 2\theta_{13}$ is 0.82×10^{-3} (90% CL, $\delta_{CP}=0$), with a 4.5 GeV beam energy and a 20 m long, 1.5 m radius decay tunnel. However, the 3.5 GeV beam may also obtain rather similar limit with 0.83×10^{-3} (90% CL) with the same tunnel parameters. The δ_{CP} independant $\sin^2 2\theta_{13}$ sensitivity is limited to $\approx 10^{-2}$ due to the $\delta_{CP} \approx 90^o$ region.

In a mixed focusing scenario, the best limit on $\sin^2 2\theta_{13}$ independent of δ_{CP} is 2.02×10^{-3} (90% CL) obtained with a 3.5 GeV beam energy and a 40 m long, 2 m radius decay tunnel.

The comparison of the optimization presented in this paper with the results obtained by other projects is displayed on figure 18. It is presented the 5 years positive focusing scenario, and two versions of a mixed scenario using positive and negative focusing: one scenario duration is 5 years in total and the other one is 10 years running in total and has been used in the previous section. It shows the complementarity of the SPL-Fréjus project with the beta beam-Fréjus project. Especially when considering the sensitivity to $\sin^2 2\theta_{13}$ for $\delta_{CP} < 0$.

The authors think that the present study may be extended in many respects. The beam line simulation part may be performed with a single simulator as FLUKA (or GEANT4 [45] for comparison). Other targets may be envisaged (tantalum, carbon) as well as other detector types as a Large Liquid Argon detector [46]. The baseline length may also be revisited as well as the off axis option. The sensitivity analysis may be deeper investigated using the complete set of possible ambiguities as in reference [17], and the θ_{13} or δ_{CP} measurement accuracy with new beam energy scenario may be investigated too.

The authors would like to thank M. Mezzetto to have expressed his interest since the early stage of this work and to have provided us with his sensitivity computation program. Also the authors thank S. Gilardoni for fruitful discussions.

A Decay probability computations

This appendix contains the probability formulas and the algorithms used in the flux computation (see section 5.1).

A.1 Pion neutrino probability computation

Pions decay only as $\pi^+ \to \mu^+ + \nu_\mu$ or $\pi^- \to \mu^- + \bar{\nu}_\mu$ and the neutrinos are emitted isotropically in the pion rest

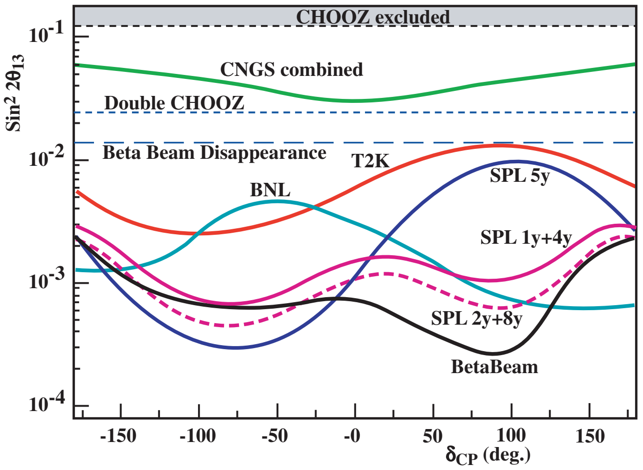

Fig. 18. 90%CL sensitivity contours labeled by the project or experiment involved. The "CHOOZ excluded" dashed curve comes from the exclusion obtained from reference [10] with $\Delta m^2 = \Delta m^2_{atm}$; in the same conditions is given the sensitivity foreseen for the "Double-CHOOZ" project [11]. The "CNGS combined" has been obtained combining the results form OPERA and ICARUS [41]. The T2K contour has been derived from reference [42]. The BNL contour has been obtained from reference [43]. The "Beta Beam" contour has been computed with 5 years running with both ν_e and $\bar{\nu}_e$ neutrino beams in an appearance mode, while the dashed "Beta Beam disappearance" has been obtained as if the β beam was analysed like a reactor experiment with 1% systematic error [44]. The "SPL 5y" and "SPL 2y+8y" and "SPL 1y+4y" curves have been obtained from the optimisation described in this paper ("5y": positive only focusing scenario; "1y+4y": 1 year of positive focusing and 4 years of negative focusing scenario; "2y+8y": 2 years of positive focusing and 8 years of negative focusing scenario) using a 3.5 GeV beam and a decay tunnel of 40 m length, and 2 m radius.

frame, with an energy of about 30 MeV given by the 2-body decay kinematics. Applying a Lorentz boost knowing the pion momentum and direction, it is possible to compute the probability to reach the detector for the neutrinos. Only neutrino parallel to the beam axis are supposed to pass through the detector fiducial area, and therefore, the neutrino must be emitted by the pion with an angle opposite to the angle between the pion and the beam axis (see figure 19). This gives:

$$\mathcal{P}_\pi = \frac{1}{4\pi}\frac{A}{L^2}\frac{1-\beta^2}{(\beta\cos\alpha - 1)^2} \tag{1}$$

where β is the velocity of the pion in the tunnel frame, A is the fiducial detector surface, L the distance between the neutrino source and the detector, and α the angle between the pion direction and the beam axis in the laboratory frame.

A.2 Muon neutrino probability computation

Muons decay only as $\mu^+ \to e^+ + \nu_e + \bar{\nu}_\mu$ or $\mu^- \to e^- + \bar{\nu}_e + \nu_\mu$, and will produce background events. The mean decay

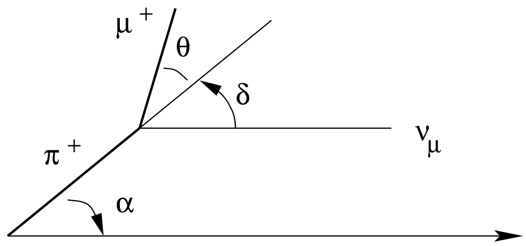

Fig. 19. Pion decay in the tunnel frame. To reach the detector, $\delta = -\alpha$ is needed.

Table 13. Flux function in the muon rest frame [47].

	$f_0(x)$	$f_1(x)$
ν_μ	$2x^2(3-2x)$	$2x^2(1-2x)$
ν_e	$12x^2(1-x)$	$12x^2(1-x)$

length of the muons is 2 km, therefore, most of them do not decay in the tunnel. This induces a lack of statistics to estimate the corresponding level of background. This problem has been solved using each muon appearing in the simulation in the following steps:

1. the probability for the muon to decay into the tunnel has been computed using a straight line propagation;
2. the available energy for the neutrino in the tunnel frame has been divided in 20 MeV energy bins;
3. one ν_e and one ν_μ have been simulated in each of the energy bins (step 2). Then, the probability to reach the detector has been computed, and multiplied by the probability computed at step (1).

After the probability computation, the non useful muon is discarded by GEANT to gain in CPU time.

The probability for the muon neutrino and the electron neutrino to be emitted parallel to the beam axis is [36]:

$$\frac{d\mathcal{P}_\mu}{dE_\nu} = \frac{1}{4\pi}\frac{A}{L^2}\frac{2}{m_\mu}\frac{1}{\gamma_\mu(1+\beta_\mu\cos\theta^*)} \times \frac{1-\beta_\mu^2}{(\beta_\mu\cos\rho - 1)^2}\left[f_0(x) \mp \Pi^L_\mu f_1(x)\cos\theta^*\right] \tag{2}$$

where β_μ and γ_μ are the velocity and the Lorentz boost of the muon in the tunnel frame, θ^* is the angle with respect to the beam axis of the muon in the muon rest frame, ρ is the corresponding angle in the tunnel frame. Like in the pion case, this angle appears because the neutrino must be parallel to the beam axis. Π^L_μ is the muon longitudinal polarization, the parameter x is defined as $x = 2E^*_\nu/m_\mu$ where E^*_ν is the neutrino energy in the muon rest frame, and the function $f_0(x)$ and $f_1(x)$ coming from the matrix element of the muon decay are given in table 13. The sign in front of Π^L_μ in equation 2 is $(-)$ for the μ^+ decays and $(+)$ for the μ^- decays, respectively.

Muon polarization is computed using the conservation of the transverse component of the velocity four-vector $\gamma(1,\beta)$ between the muon rest frame (where the polarization is computed) and the pion rest frame, where the

Table 14. Charged and neutral kaon decay channels [49].

$K^{\pm}$		K_L^0		K_S^0	
$\mu^{\pm}\nu_{\mu}$	63.51%	$\pi^-e^+\nu_e$	19.35%	$\pi^+\pi^-$	68.61%
$\pi^{\pm}\pi^0$	21.17%	$\pi^+e^-\bar{\nu}_e$	19.35%	$\pi^0\pi^0$	31.39%
$\pi^{\pm}\pi^+\pi^-$	5.59%	$\pi^-\mu^+\nu_{\mu}$	13.5%		
$e^{\pm}\nu_e\pi^0$	4.82%	$\pi^+\mu^-\bar{\nu}_{\mu}$	13.5%		
$\mu^{\pm}\nu_{\mu}\pi^0$	3.18%	$\pi^0\pi^0\pi^0$	21.5%		
$\pi^{\pm}\pi^0\pi^0$	1.73%	$\pi^+\pi^-\pi^0$	12.38%		

muon helicity is -1, due to the parity non conservation. It yields [48]:

$$\Pi_{\mu}^{T} = \frac{\gamma_{\pi}\beta_{\pi}}{\gamma_{\mu}\beta_{\mu}} \sin\theta^* \text{ and } \Pi_{\mu}^{L} = \sqrt{1-\Pi_{\mu}^{T2}} \quad (3)$$

where γ_{π}, β_{π}, γ_{μ}, and β_{μ} are the Lorentz boost and velocity of the pion and of the muon in the tunnel frame, and θ^* the angle with respect to the beam axis of the muon in the pion rest frame.

A.3 The treatment of the kaons

Contrary to pions and muons, kaons have many decay channels. They are summarized in table 14.

There is a very small amount of kaons produced (section 3), and this number has been artificially increased in order to obtain statistically significant results. The multiplicity of decay channels makes impossible the method used for the muon case (A.2). The method chosen for the good compromise between the gain in CPU and the statistical uncertainty of the results, is to duplicate many times each kaon exiting the target. The number of duplication varies between 10 and 300. It depends on the initial kaon rate and therefore on the beam energy.

All the kaons daughter particles are tracked by GEANT until they decay. Three different types of daughter particles are identified in the kaon decays. The first type corresponds to primary neutrinos, the second type concerns charged pions and muons, and the neutral pions are left for the last type.

In the $K^{\pm} \to \mu^{\pm}\nu_{\mu}(\bar{\nu}_{\mu})$ decay modes, the computation of the probability for a neutrino to reach the detector is the same than the 2-body decay formula used to in the pion decay (equation 1), where β is now the kaon velocity, and α the angle of the kaon with respect to the beam axis.

When a neutrino is produced by a kaon 3-body decay, the probability to reach the detector is computed using a pure phase space formula. It yields:

$$\begin{aligned}\mathcal{P}_K = & \frac{1}{4\pi}\frac{A}{L^2}\frac{1}{m_K - m_{\pi} - m_l} \\ & \times \frac{1}{\gamma_K(1+\beta_K\cos\theta^*)}\frac{1-\beta_K^2}{(\beta_K\cos\delta - 1)^2} \end{aligned} \quad (4)$$

where m_K is the kaon mass (charged or neutral), m_{π} is the pion mass (π^0 mass in $K^{\pm}$ decays and $\pi^{\pm}$ mass in K_L^0 decays), and m_l is the mass of the lepton associated with the neutrino. The β_K and γ_K are the velocity and the Lorentz boost of the kaon, θ^* is the angle between the neutrino direction and the kaon direction, in the kaon rest frame. Finally, δ is the angle between the kaon direction and the beam axis in the tunnel frame.

When a $\pi^{\pm}$ is produced in the kaon decay chain, it is tracked by GEANT until it decays, and the probability of equation 1 is applied to the produced neutrino. In case of a muon, it is treated as explained in A.2. The muon polarization is computed this time using the kaon decay informations. Finally, when a π^0 is produced, as it cannot create neutrinos, it is simply discarded.

References

1. E. Kearns [SuperKamiokande Collaboration], talk at the International Conference NEUTRINO 2004, 14-19 June 2004, http://neutrino2004.in2p3.fr/
2. T. Nakaya [K2K Collaboration], *Nucl. Phys.* B (Proceedings Supplement) **143**, 96 (2005)
3. T. Thomson [MINOS Collaboration], *Nucl. Phys.* B (Proceedings Supplement) **143**, 249 (2005); P. Adamson et al., NuMi-L-337 (unpublished)
4. D. Autiero [OPERA Collaboration], *Nucl. Phys.* B (Proceedings Supplement) **143**, 257 (2005); M. Guler et al., *Experiment proposal* CERN/SPSC 2000-028 SPSC/P318 LNGS P25/2000 (unpublished)
5. A. Bueno [ICARUS Collaboration], *Nucl. Phys.* B (Proceedings Supplement) **143**, 262 (2005); P. Aprili et al., CERN-SPSC-2002-027 (unpublished)
6. G. Acquistapace et al., CERN-98-02 (unpublished)
7. A. Athanassopoulos et al., *Phys. Rev. Lett.* **81**, 1774 (1998); A. Aguilar et al., *Phys. Rev.* D **64**, 112007 (2001)
8. I. Stancu et al., FERMILAB-TM-2207 (unpublished)
9. B. Pontecorvo *Sov. Phys.–JETP* **6**, 429 (1957) [*Zh. Eksp. Teor. Fiz.* **33**, 549 (1957)]; Z. Maki, M. Nakagawa and S. Sakata *Prog. Theor. Phys.* **28**, 870 (1962); Pontecorvo B *Sov. Phys.–JETP* **26**, 984 (1968) [*Zh. Eksp. Teor. Fiz.* **53**, 1717 (1967)]; V. N. Gribov and B. Pontecorvo *Phys. Lett.* B **28**, 493 (1969)
10. M. Apollonio et al., *Phys. Lett.* B **466**, 415 (1999); M. Apollonio et al., *Eur. J. Phys.* C **27**, 331 (2003)
11. K. Anderson et al., *White paper report on using nuclear reactors to search for a value of* θ_{13} (2004), http://www.hep.anl.gov/minos/reactor13/reactor13.pdf (unpublished); F. Arbelier et al., *Letter of Intend for Double-CHOOZ*, arXiv:hep-ex/0405032 (unpublished)
12. P. Zucchelli, *Phys. Lett.* B **532**, 166 (2002)
13. I. Ambats et al., NOνA proposal FNAL P929, 2004 (unpublished)
14. Y. Itow, KEK report 2001-4, ICRR-report-477-2001-7, TRI-PP-01-05 (unpublished), see also arXiv:hep-ex/0106019
15. M. V. Diwan, *Phys. Rev.* D **68**, 012002 (2003)
16. A. Blondel et al., CERN-2004-002 (unpublished)
17. A. Donini et al., IFT-UAM/CSIC-04-30, 2004 (unpublished); see also arXiv:hep-ph/0406132
18. F. Dalnoki-Veress, the Double-CHOOZ project arXiv:hep-ex/0406070 (unpublished)
19. B. Autin et al., CERN-2000-12 (unpublished)

20. The UNO whitepaper, *Physics Potential and Feasibility of UNO*, SBHEP01-3 (unpublished), see also http://ale.physics.sunysb.edu/uno/
21. L. Mosca, Talk at the Physics with a Multi MegaWatt Proton Source Workshop at CERN 25-27 May 2004, see http://physicsatmwatt.web.cern.ch/physicsatmwatt/
22. S. van der Meer, CERN-Report No 61-7, 1961 (unpublished)
23. J.E. Campagne and A. Cazes, CERN-NUFACT-Note-134, 2003 (unpublished), see http://slac.web.cern.ch/slap/NuFact/NuFact/NFNotes.html
24. J.E. Campagne and A. Cazes, Poster session at the Physics with a Multi MegaWatt Proton Source Workshop at CERN 25-27 May 2004, see http://physicsatmwatt.web.cern.ch/physicsatmwatt/
25. J.J. Gómez Gadenas et al., IFIC/01-31, Proceedings of Venice 2001, Neutrino telescopes, vol. 2, p463-481; see also arXiv:hep-ph/0105297; A. Blondel et al., *Nucl. Instrum. Methods* A **503** 173 (2001); A. Blondel et al., CERN-2004-002
26. M. Mezzetto, *J. Phys. G: Nucl. Part. Phys.* **29**, 1781-1784 (2003), see also arXiv:hep-ex/0302005
27. J.E. Campagne, CERN-NUFACT-Note-138, 2004 (unpublished), see http://slap.web.cern.ch/slap/NuFact/NuFact/NFNotes.html
28. A. Fasso et al., Proceedings of the MonteCarlo 2000 conference, Lisbon, October 26 2000, A. Kling et al.- eds., Springer-Verlag Berlin, p159-164 (2001); A. Fasso et al., Proceedings of the MonteCarlo 2000 conference, Lisbon, October 26 2000, A. Kling et al.- eds., Springer-Verlag Berlin, p955-960 (2001)
29. R. Garoby, Talk at the Physics with a Multi MegaWatt Proton Source Workshop at CERN 25-27 May 2004, http://physicsatmwatt.web.cern.ch/physicsatmwatt/
30. C. Catanesi et al., CERN-SPSC 2002/019 (unpublished)
31. D. Drakoulakos et al., Fermilab P-938 (unpublished), see also arXiv:hep-ex/405002
32. N.V. Mokhov et al., The MARS Code System User Guide, Version 13(95), Fermilab-FN-628 (1995); N.V. Mokhov et al., MARS oed Develepments, LANL Report LA-UR-98-5716 (1998), nucl-th/9812038 v2 16 December 1998, http://www-ap.fnal.gov/MARS/
33. G. Battistoni and A. Ferrari, *private communication*
34. Application Software group, Computing and Network Division et al.GEANT Description and Simulation Tool, CERN Geneva, Switzerland
35. S. Gilardoni, Talk at NuFact03 (2003), see http://www.cap.bnl.gov/nufact03/
36. A. Blondel et al., CERN-NUFACT-Note-78, 2001 (unpublished), see http://slap.web.cern.ch/slap/NuFact/NuFact/NFNotes.html
37. M. Mezzetto, CERN-NUFACT-Note-60, 2000 (unpublished), see http://slap.web.cern.ch/slap/NuFact/NuFact/NFNotes.html
38. A. Donini, D. Meloni and S. Rigolin, J. High Energy Phys. **0406**, 011 (2004), see also arXiv:hep-ph/0312072
39. D. Casper, *Nucl. Phys. Proc. Suppl.* **112**, 161-170 (2002), see also arXiv:hep-ph/0208030
40. G. Gratta, talk at the International Conference NEUTRINO 2004, 14-19 June 2004, http://neutrino2004.in2p3.fr/
41. M. Komatsu, P Migliozzi and F. Terranova, *J. Phys. G: Nucl. Part. Phys.* **29**, 443 (2003); see also arXiv:hep-ph/0210043
42. T. Kobayashi, *Nucl. Phys.* B (Proceedings Supplement) **143**, 303 (2005)
43. M.V. Diwan et al., *Phys. Rev.* D **68**, 012002 (2003); see also figure 8 of arXiv:hep-ph/0303081
44. M. Mezzetto, *private communication*: the corresponding θ_{13} limit is 3.4^o.
45. A. Agostinelli et al., *Nucl. Instrum. Methods* A **506**, 250-503 (2003)
46. A. Ereditato and A. Rubia, Talk at the Physics with a Multi MegaWatt Proton Source Workshop at CERN 25-27 May 2004, see http://physicsatmwatt.web.cern.ch/physicsatmwatt/
47. T.K. Gaisser, *Cosmic Rays and Particle Physics* (Cambridge University Press, 1990)
48. F. Combley and E. Picasso, *Phys. Rept.* **14**, 1 (1974)
49. K. Hagiwara et al., *Phys. Rev.* D **66**, 010001 (2002)